ACS OMEGA

http://pubs.acs.org/journal/acsodf

Article

Revealing the Chemical Nature of Functional Groups on Graphene Oxide by Integrating Potentiometric Titration and Ab Initio Calculations

Wuqing Tao, Youshi Lan, Jiqiao Zhang, Liyang Zhu, Qian Liu, Yating Yang, Suliang Yang,* Guoxin Tian, and Shengdong Zhang*

Cite This: *ACS Omega* 2023, 8, 24332−24340

Read Online

ACCESS | Metrics & More | Article Recommendations | Supporting Information

ABSTRACT: A new graphene oxide (GO) model with reasonable functional group types and distribution modes was proposed by integrating potentiometric titrations and ab initio calculations. Due to the complex synthesis mechanism, the atomic structure of GO has been controversial for a long time. Here, we use density functional theory calculations to mimic the oxidation process, and a series of GO fragments (GOFs) were deduced. A new pK_a calculation method (RCDPKA) developed specifically in this work was further used to predict pK_a values of the fragments. Then, we performed potentiometric titrations on four different GO samples to confirm the existence of these GOFs and determine the content of functional groups. Interestingly, different GO samples present the same pK_a values in titration, and the results are consistent with the predicted ones. Based on the evidence from titration and calculation, prominent correlations between functional groups could be found. Groups at the edges are mainly double-interactive carboxyls (pK_{a1} ≈ 3.4, pK_{a2} ≈ 5.7) and double-adjacent phenolic hydroxyls (pK_{a1} ≈ 8.8, pK_{a2} ≈ 12.1), while groups on the plane are mainly collocated epoxies and hydroxyls (pK_{a1} ≈ 11.1, pK_{a2} ≈ 13.8) on both sides of the plane with a meta-positional hydrogen bond interaction. These findings were further validated by multiple characterizations and GO modifications. These results not only stimulate a fundamental understanding of the GO structure but also provide a quantitative analysis method for functional groups on GO.

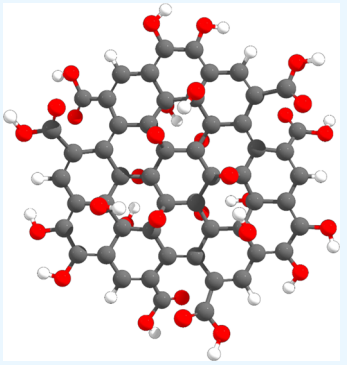

1. INTRODUCTION

Graphene oxide (GO), a branch of graphene-based functional materials, has attracted tremendous attention in the field of materials science.[1,2] GO possesses abundant oxygen-containing functional groups, a large surface area, and excellent hydrophilicity, making it an important matrix material,[2] aqueous adsorbent,[3] and promising precursor for large-scale production of graphene.[4] However, currently, the underlying mechanism for the formation and precise atomic structure of GO remains uncertain.[5] This is primarily due to the diversity of oxidation routes, non-stoichiometry of oxidized products, and limitation of characterization techniques.[6] Multiple routes have been reported for preparing GO with different oxidants, such as Brodie,[7] Staudenmaier,[8] Hofmann,[9] Hummers,[10] and Tour[11] methods. Also, at least six conflicting models have been proposed to elucidate the structural features of GO, including Hofmann−Holst,[12] Ruess,[13] Scholz−Boehm,[14] Nakajima−Matsuo,[15] Lerf−Klinowski,[16] and Szabó−Dékány[17] models (Figure 1). These models contain contradictory information, which makes us more confused with the GO structure.[18] Recent studies employed various intensive techniques including ^{13}C and ^{1}H nuclear magnetic resonance spectroscopy,[19] transmission electron microscopy,[20] X-ray photoelectron spectroscopy (XPS),[21] X-ray adsorption spectroscopy,[22] X-ray absorption near-edge spectroscopy,[23] Fourier transform infrared spectroscopy (FT-IR),[24] Raman spectroscopy,[25] and density functional theory (DFT) calculations[26,27] to provide more direct information. As commonly accepted now, GO is a material with a roughly 2:1 C/O ratio and with a rugged surface randomly covered with oxidized and unoxidized regions. The unoxidized regions retain some graphene-like properties, while the oxidized regions are randomly decorated by adjacent hydroxyl and epoxy groups up and down because of the hydrogen bonds and steric hindrances. The edge of GO is surrounded by phenolic and carboxyl groups and perhaps accompanied by a small amount of carbonyl, quinone, and lactone groups.[28] However, there is little information about the distribution relationship between functional groups.

Insight into the GO structure properties is of significance for mastering its mechanism of function and further modification.[29] Here, we adopt both computational and experimental methods to further identify the atomic structure and

Received: March 9, 2023
Accepted: May 29, 2023
Published: June 29, 2023

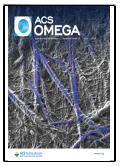

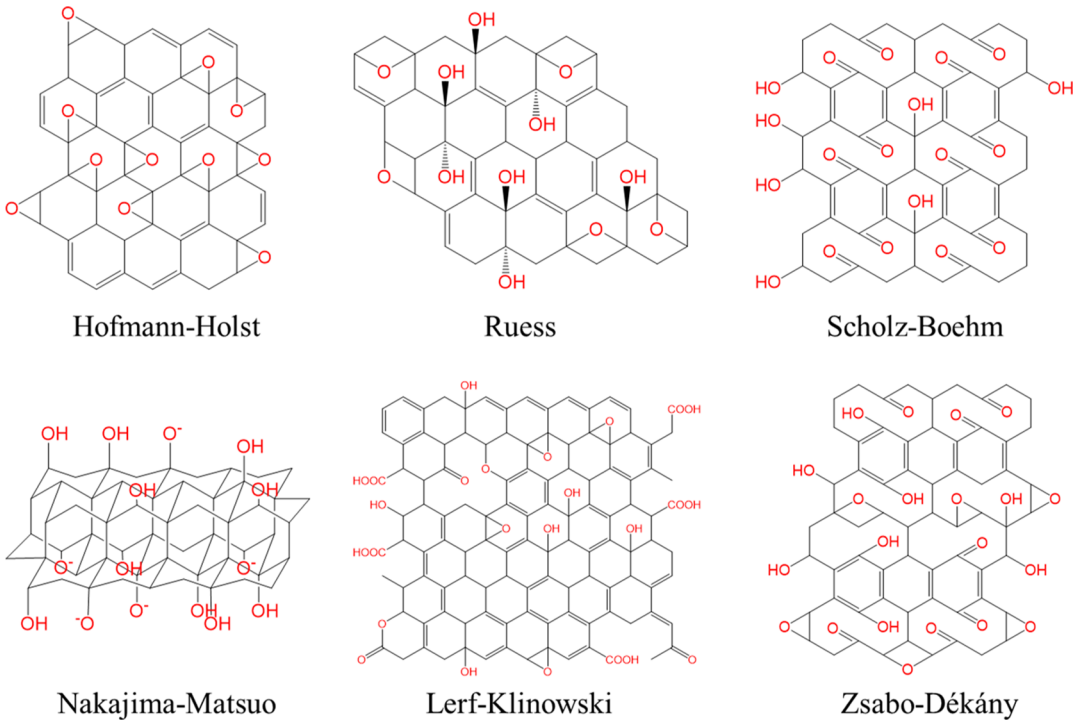

Figure 1. Six proposed GO models.

quantitively analyze the oxygen-containing functional groups of GO. DFT calculation was first conducted to search for the possible oxygen-containing groups at the plane and edge of GO. Then, a new pK_a prediction method [refined comparative dissociation free energy methods for pK_a (RCDPKA)] was proposed to estimate the pK_a values of each group. pK_a values of different GO samples were also obtained by potentiometric titration of the aqueous suspensions of GO with a standard NaOH solution. By comparing the simulation and titration results, species and dissociable contents of the functional groups can be obtained, and a new GO model that can reflect the distribution relationship among functional groups can also be proposed. Furthermore, four different modification procedures were conducted on GO, and the same analysis process was performed on the modified samples, which consistently reflect our results.

2. METHODS

2.1. GO Samples. Four GO samples, CCTGO-204 (aqueous suspension of ∼3 μm-sized GO, Beijing Carbon Century Technology Co., Ltd.), CCTGO-104 (∼3 μm-sized GO flakes, Beijing Carbon Century Technology Co., Ltd.), GO-V20 (18−104 μm-sized GO flakes, D50 = 50 μm, 1.1−1.3 nm thickness, Standard Graphene Co., Ltd.), and GO-V50 (20−167 μm-sized GO flakes, D50 = 65 μm, 1.1−1.3 nm thickness, Standard Graphene Co., Ltd.), were used in this work.

2.2. Potentiometric Titration. Potentiometric titrations of the GO samples were performed using an automatic potentiometric titrator (907 Titrando, Metrohm Co., Ltd.) equipped with a pH glass electrode (PT-1000, Metrohm Co., Ltd.). The glass electrode was calibrated by means of a strong acid−strong base titration using the GLEE program. The pK_a values of GO were estimated from the titration of the GO suspension with a standard NaOH solution using HyperQuad 2008[30] as the fitting program. All solutions were made with "CO2 free" water. This milliQ water (resistivity > 18 MΩ·cm) was boiled and cooled under a stream of nitrogen. All potentiometric titrations were conducted in a 0.1 mol/L $NaClO_4$ solution in a 25.0 ± 0.1 °C water bath under argon protection and repeated at least twice. For a typical titration of the GO sample, the pH value of 20 mL of a 0.1 mol/L $NaClO_4$ solution containing 20 mg of GO, the initial solution in the titration cell, was adjusted to ∼2.5 with a certain amount of $HClO_4$ before the titration. The titrant was usually 0.1038 mol/L NaOH.[43]

2.3. GO Modifications. *2.3.1. Preparation of CCTGO-204-HNO_3.* The mixture of 40 mL of GO suspension (CCTGO-204, 5 mg/mL), 40 mL of HNO_3 (65%), and 20 mL of deionized water was heated during refluxing at 130 °C for 4 days under vigorous magnetic stirring. During the reaction process, three drops of anhydrous ethanol were added 32 times at regular time intervals to promote the oxidation. The supernatant was discarded after 3 min of centrifugation at 6000 rpm. After washing with deionized water and discarding the supernatant twice, the acquired GO material was transferred into a dialysis bag (MD44-3.5, MWCO 3500, Viskase) placed in a large volume of deionized water. The deionized water was replaced repeatedly until the pH value of the solution outside the bag increased to near neutral.

2.3.2. Preparation of CCTGO-204-HCl. The mixture of 40 mL of concentrated HCl and 40 mL of GO suspension (CCTGO-204, 5 mg/mL) was heated during refluxing at 125 °C for 4 days under vigorous magnetic stirring. Then, the same centrifugation, washing, and dialysis procedures for the preparation of CCTGO-204-HNO_3 were employed to get CCTGO-204-HCl.

2.3.3. Preparation of CCTGO-204-COOH. 5.0 g of NaOH solid was added into the mixture of 40 mL of GO suspension (CCTGO-204, 5 mg/mL) and 60 mL of deionized water. After 30 min of stirring, 7.0 g of $ClCH_2COONa$ was added and 6 h of ultrasonic treatment was followed. After 12 h of standing, 20

https://doi.org/10.1021/acsomega.3c01596
ACS Omega 2023, 8, 24332−24340

mL of concentrated HNO_3 was added dropwise for neutralization. Then, the same centrifugation, washing, and dialysis procedures as for the preparation of CCTGO-204-HNO_3 were employed to get CCTGO-204-COOH.

2.3.4. Preparation of CCTGO-204-HNO_3-COOH. CCTGO-204-HNO_3-COOH, a carboxylation product of CCTGO-204-HNO_3, was prepared by following the same procedures used for the preparation of CCTGO-204-COOH.

2.4. DFT Calculations. DFT calculations were performed by using B3LYP[31,32]/TZVP[33,34] as implemented in Gaussian 09.[35] Geometry and electronic structure optimizations were carried out in the aqueous phase with no constraints imposed beyond the multiplicity of the electronic state. Based on the optimized structures, frequency calculations were performed to determine the thermodynamic free energy of each structure at the same level of theory. All computed structures were local minima with no imaginary frequencies. The aqueous solution effect and the dispersion correction were considered by introducing the SMD[36] continuum solvent model and Grimme's D3(BJ)[37] model, respectively.

3. RESULTS

The synthesis routes of GO are multiple and complex and the current oxidation mechanism of GO is mainly based on

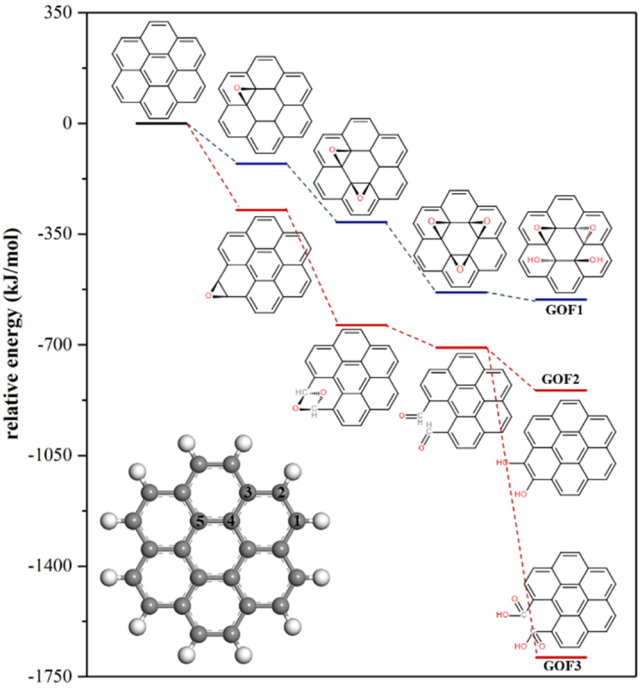

Figure 2. Oxidation process of graphene. The coronene mimics the mono layer graphene, and the active oxygen and water are oxidants implicit in the surrounding. The ball and stick model of coronene is displayed at the bottom left with reaction sites marked on the carbon atoms. The blue lines represent the oxidation process on the plane, while the red line represents the oxidation process at the edge. For better comparison, the DFT energy summation of one coronene, four active oxygen atoms, and one water molecule is set to zero.

conjecture. As commonly accepted, the oxidation process of GO mainly comprised three stages: intercalation by acids (fuming HNO_3 and concentrated H_2SO_4), oxidation by oxidants ($KClO_3$ and $KMnO_4$), and exfoliation by water. Considering that all the adopted oxidants can produce active

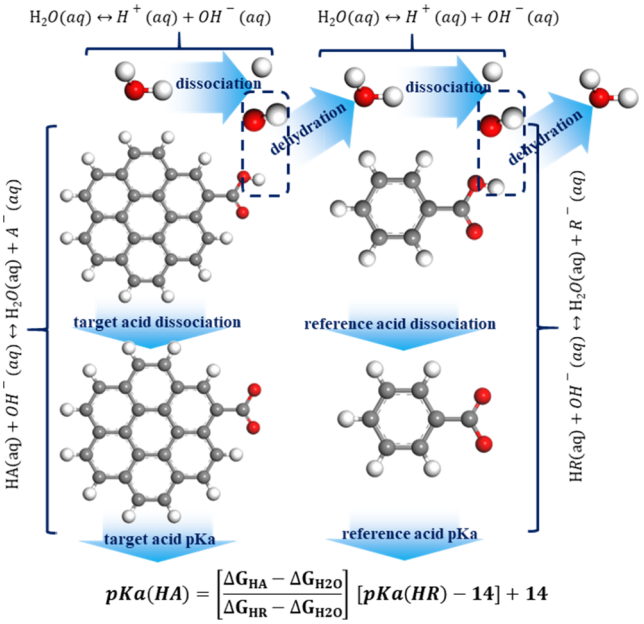

Figure 3. Calculation scheme of RCDPKA. HA represents the target acid with unknown pK_a, while HR represents the reference acid with known pK_a. The gray, white, and red spheres represent the carbon, hydrogen, and oxygen atoms.

oxygen and all preparation routes involve water exfoliation, we take the oxygen radical and water as the main oxidants in our calculations. As shown in Figure 2, coronene is adopted to imitate graphene, and the oxidation processes on the plane and edge were investigated separately to obtain the GO fragments (GOFs). Calculation results show that the oxygen radical is inclined to be attached with the sp2 hybrid carbon (site 1) connecting with the hydrogen atom at the edge of graphene and spontaneously combined with the second sp2 hybrid carbon (site 2) to form an epoxy. The oxygen radical is not inclined to form an epoxy between sites 2 and 3, which indicates that carbons on the edge of GO are active than that on the plane.[38,39] With the formation of the second epoxy between sites 1 and 2 on the opposite side, the single bond between two carbon atoms breaks to form dialdehyde, which can either be re-cyclized to form catechol (GOF2) or further be oxidized to form the dicarboxylic group (GOF3) to lower the overall energy. Oxidation on the plane also starts with the formation of epoxy on both sides of GO. Similar to the oxidation process at the edge, epoxy inclines to form between sites 4 and 5 rather than sites 3 and 4. Our study finds that epoxies are inclined to locate adjacent to the previous ones, which is consistent with the fact that oxygen-containing functional groups are relatively concentrated on the plane of GO.[26,40] Considering that there are no hydrogen atoms on the plane of GO, the main product of the oxidation process should only be epoxy, while the hydroxyl was produced in the water exfoliation process, where one water molecule can react with one epoxy to form two hydroxyls, which leads to the hydroxyls on the GO surface appearing in pairs. Experimental findings show that the conformations of epoxy and hydroxyl on the plane are not static[41,42] but interchangeable in the aqueous solution. Thus, the conformation energy of the oxidized region decorated by only epoxy should get very close to that of the region decorated by both epoxy and hydroxyl under an aqueous solution environment. For satisfying this condition,

https://doi.org/10.1021/acsomega.3c01596
ACS Omega 2023, 8, 24332−24340

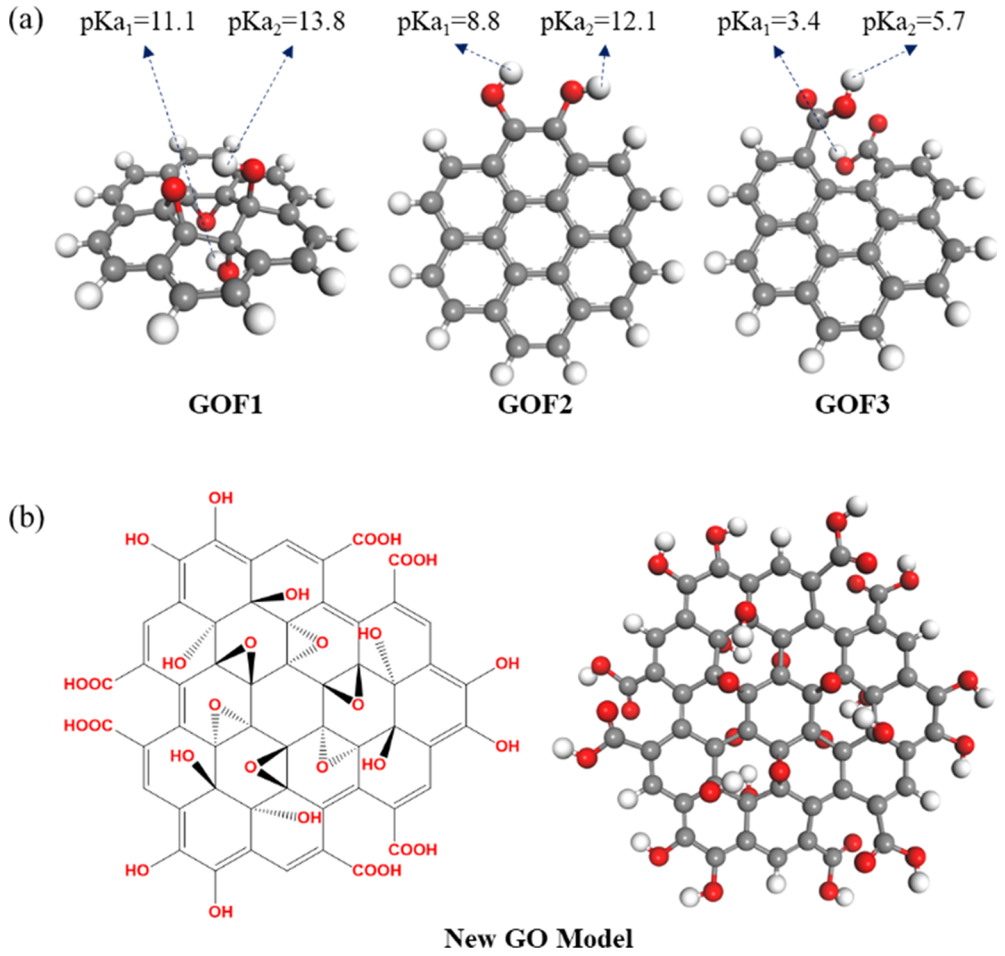

Figure 4. (a) Atomic structure of GOFs and corresponding pK_a values. (b) Our new proposed GO model by assembling GOFs and with a central carbon ring in the highest oxide state. The gray, white, and red spheres represent the carbon, hydrogen, and oxygen atoms.

Table 1. Protonation Constants and Species Contents of Four Different GO Samples

	CCTGO-204	CCTGO-104	GO-V50	GO-V20
		Log β (pK_a)		
HA	3.90	3.95	3.82	3.76
HB	6.26	6.36	6.09	5.66
HC	8.42	8.54	8.57	8.61
HD	10.38	10.43	10.68	10.57
		Total Content (mmol/g)		
A	0.89	0.76	0.79	0.60
B	0.89	0.83	0.62	0.41
C	1.07	0.85	1.15	1.27
D	1.54	1.37	1.74	1.60

the ratio of epoxy and hydroxyl in our model is determined as 2:2 (as can be seen from Figure 2, the relative energy of GOF1 is very close to that of its precursor.), and the energy-favorable structure is obtained by screening its eleven distinguished conformations (Table S1). The result shows that the same type of functional groups on the plane tend to be adjacent on the opposite surface, and the hydroxyl is inclined to locate at the meta-position to the epoxy interacting with each other by a hydrogen bond.

To confirm the existence of these GOFs, their pK_a values are obtained by both the theoretical method and potentiometric titration for a precise comparison. There are several methods to predict the pK_a value from the atomic structure, such as thermodynamic cycle calculation,[40] electrostatic potential fitting,[44] proPka program,[45] and H++ software.[46] However, they do not meet our requirement here for both high accuracy and large molecular size. Herein, we propose a new route to obtain the pK_a value with the aid of DFT calculations, named RCDPKA. Our route gained a lot of inspiration from the relative free energy method proposed by Zeng's group,[47] which introduced two reference acids to eliminate the systematic errors. Based on this, we further considered that the dissociation of the acid in the aqueous solution is driven by water dissociation, in which the hydroxyl ions released from water took away the protons from the acid. Furthermore, an analogous acid with a small atomic structure and known pK_a value should be selected as the reference. Such treatments can diminish both the influences from proton dissociation and systematic error. The calculation scheme of RCDPKA is displayed in Figure 3, and the accuracy has been validated by calculating several pK_a-known acids (Table S2). RCDPKA was further employed to predict the pK_a value of each inferred GOF. Since the same type of functional groups are adjacent to each other and close to the aromatic carbon, catechol and phthalic acid are selected as the references for hydroxyl and carboxyl pK_a calculations, respectively. As shown in Figure 4a, GOF1 containing two adjacent hydroxyls, respectively, interacting with meta-positional epoxies on the opposite surface has two levels of pK_a values, 11.1 and 13.8. Similarly,

https://doi.org/10.1021/acsomega.3c01596
ACS Omega 2023, 8, 24332−24340

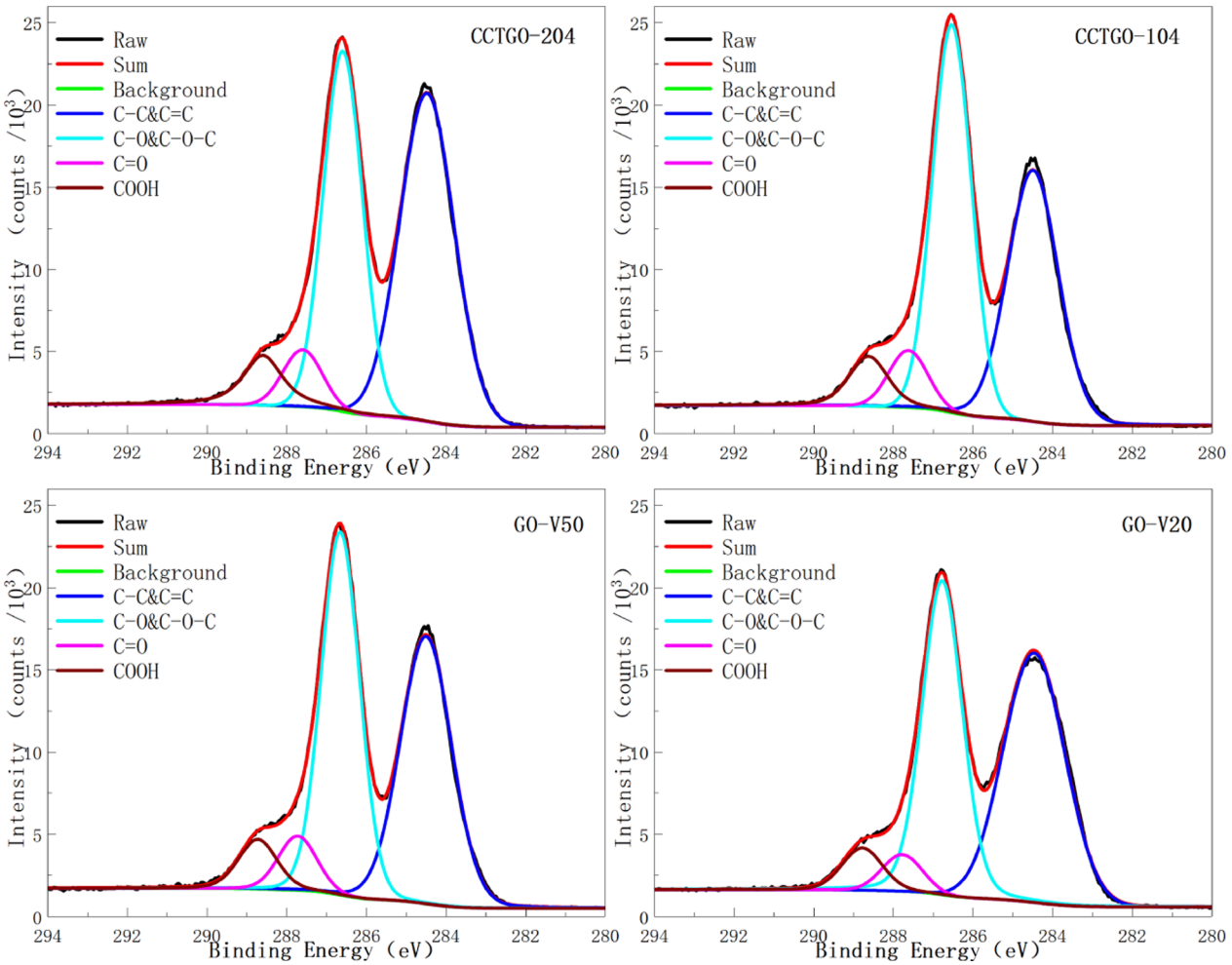

Figure 5. C1s-XPS of the original GO samples. Six kinds of carbon connection modes can be distinguished from C 1s-XPS spectra, including C−C, C═C, C−O, C−O−C, C═O, and O═C−OH. Fitting results show that the relative content of O═C−OH for the four original GO samples is CCTGO-204 > CCTGO-104 > GO-V50 > GO-V20.

Figure 6. Appearance of CCTGO-204, CCTGO-204-HNO_3, CCTGO-204-COOH, CCTGO-204-HNO_3-COOH, and CCTGO-204-HCl (denoted as GO, HNO_3, COOH, HNO_3−COOH, and HCl in the image, respectively) with the same concentration of GO.

GOF2 containing double-adjacent phenolic groups at the edges leads to two levels of pK_a values, 8.8 and 12.1. GOF3 containing two adjacent-interactive carboxyl groups results in two diverse pK_a values, 3.4 and 5.7. More details of the pK_a calculation for GOF can be seen from Table S3.

To validate the calculation results, potentiometric titration was performed on four GO samples (CCTGO-204, CCTGO-104, GO-V50, and GO-V20), and the results are fitted with the HyperQuad 2008 program to obtain the content of oxygen-containing functional groups and corresponding pK_a values (Figure S1 and Table 1). As can be seen from the fitting results, the proton dissociation behaviors of the samples are very similar during the titration experiments. Four-level deprotonations are detected for each sample, denoted as HA, HB, HC, and HD. The pK_a values are almost equal for different samples, roughly 3.8, 6.0, 8.5, and 10.5, which indicates that these different GO samples possess the same kinds of functional groups on the surface. The content of the groups of different sample varies a lot but generally present a regular pattern of D > C > A ≥ B. Thus, we may infer that A and B are two interdependent species, while C and D species are dominant on the GO surface.

As can be seen from Table 1, the different GO samples may have different contents of groups, but the main species of functional groups stay the same. This viewpoint can also be supported by FT-IR characterizations (Figure S4). By comparing the calculation and the titration results, the atomic structure of functional groups can be distinguished. The interdependent A and B species have pK_a values of 3.8 and 6.0, corresponding to the double adjacent carboxylic group of GOF1 (pK_{a1} = 3.4 and pK_{a2} = 5.7). From this point of view, the contents of A and B should be strictly equal. However, GO is the amorphous sheet with corner and irregular defect. Thus, fluctuation can be observed from the results. The pK_a value of C species is about 8.5, corresponding to the first-level

https://doi.org/10.1021/acsomega.3c01596
ACS Omega 2023, 8, 24332−24340

Table 2. Protonation Constants and Species Contents of Four Modified GOs

	CCTGO-204-HNO_3	CCTGO-204-COOH	CCTGO-204-HNO_3-COOH	CCTGO-204-HCl
		Log β (pK_a)		
HA	3.81	3.76	3.54	3.99
HB	6.11	5.70	5.37	6.04
HC	8.56	7.96	7.73	8.40
HD	10.71	10.08	10.03	10.56
		Total Content (mmol/g)		
A	1.49	1.29	1.89	0.93
B	1.02	1.09	1.49	0.89
C	1.30	0.87	0.98	0.84
D	2.35	1.10	1.61	1.34

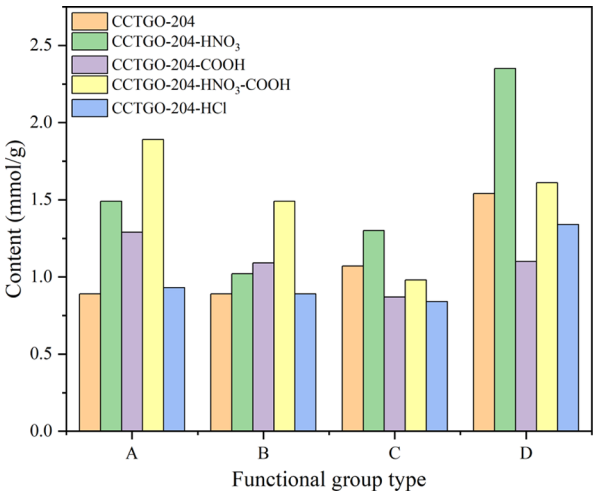

Figure 7. Functional group content comparison between CCTGO-204 and its four modified samples where A and B denote the two carboxyl groups on GOF3; C denotes the phenolic hydroxyl group on GOF2; and D denotes the alcoholic hydroxyl groups on GOF1.

dissociation of GOF2 (pK_{a1} = 8.8 and pK_{a2} = 12.1), while the pK_a value of D species is about 10.5, corresponding to the first-level dissociation of GOF3 (pK_{a1} = 11.1 and pK_{a2} = 13.8). The second-level dissociation of C and D is out of our titration ranges. All fitting results show that the content of D is larger than that of C, indicating that the hydroxyl groups on the plane are more dominant than the phenolic groups at the edge, which also can be validated by XPS analysis (Figure 5). Thus, the main species of oxygen-containing functional groups distinguished by our calculations is consistent with the experimental characterizations, and the dissociable content of each group obtained in our potentiometric titrations is also reliable. By assembling the deduced GOFs and making the central carbon ring in the highest oxide state, a new GO model that can better reflect the distribution relationship between functional groups is proposed as shown in Figure 4b.

These results not only promote our understanding on the structure of GO but also provide an approach to detect the changes in the modifications. Here, we select CCTGO-204 as the candidate for four different modification procedures: oxidation by 6 M HNO_3 (CCTGO-204-HNO_3), carboxylation by Cl−CH_2−COONa (CCTGO-204-COOH), carboxylation by Cl−CH_2−COONa after oxidation by HNO_3 (CCTGO-204-HNO_3-COOH), and acidification by 6 M HCl (CCTGO-204-HCl). The appearances of these four modified materials and the original sample with the same concentrations are displayed in Figure 6. As can be seen, the color of the CCTGO-204-HNO_3 suspension is lighter and the transparency is higher than that of CCTGO-204, while the others become darker, which means that CCTGO-204-HNO_3 possesses better dispersibility. The color of CCTGO-204-COOH is similar to that of CCTGO-204-HNO_3-COOH, but the aqueous dispersibility of CCTGO-204-COOH is worse, with a small number of particles adhered to the glass wall. Surprisingly, the suspension of CCTGO-204-HCl displays extremely poor aqueous dispersibility, with a large number of particles separated out. These phenomena are also confirmed by SEM (Figure S3) showing that modification can greatly change the smoothness of the GO surface: CCTGO-204-HNO_3 > CCTGO-204 > CCTGO-204-NHO_3-COOH > CCTGO-204-COOH > CCTGO-204-HCl.

To understand the influence of different modification procedures on GO, we perform the same titration process on the modified samples and use the same species classification to fit the titration results (Figure S2 and Table 2). As can be seen, modifications scarcely change the pK_a values, implying that the main species of functional groups stay unchanged, which also can be supported by the FT-IR characterizations (Figure S5). For CCTGO-204-HNO_3, CCTGO-204-COOH, and CCTGO−HNO_3−COOH, the four-level pK_a values show a slightly decreasing trend, indicating that the acidity of GO is gradually increased, which also means that these three treatments can effectively increase the content of proton-dissociable functional groups. The concentrated HNO_3 can further oxidize the GO sample, which leads to an increasement of the content of carboxyl and hydroxyl groups, while Cl−CH_2−COONa can increase the content of carboxyl groups by consuming hydroxyl and epoxy groups. The content variation of each functional group (Figure 7) results in corresponding modification reactions, indicating that our species' classification and titration can describe in detail the changes that occurred on GO. However, there is a contradiction between titration results and suspension dispersibilities. According to titrations, the order of the total contents of functional groups is CCTGO-204-HNO_3 > CCTGO-204-HNO_3-COOH > CCTGO-204-COOH > CCTGO-204, which is inconsistent with the rank of dispersibilities. Moreover, CCTGO-204-HCl bears an unexpectedly poor dispersibility after being treated by concentrated HCl. For validating the correctness of our titration, XPS (Figure 8) and elemental analysis (Table S4) are further adopted. As can be seen from C 1s-XPS, the content of carboxyl displays a rank of CCTGO-204-HNO_3-COOH > CCTGO-204-HNO_3 ≈ CCTGO-204-COOH > CCTGO-204-HCl, which is consistent with our titration. The peaks related to the total content of C−O and C−O−C decreased evidently in all samples, indicating that a large number of epoxies are

https://doi.org/10.1021/acsomega.3c01596
ACS Omega 2023, 8, 24332−24340

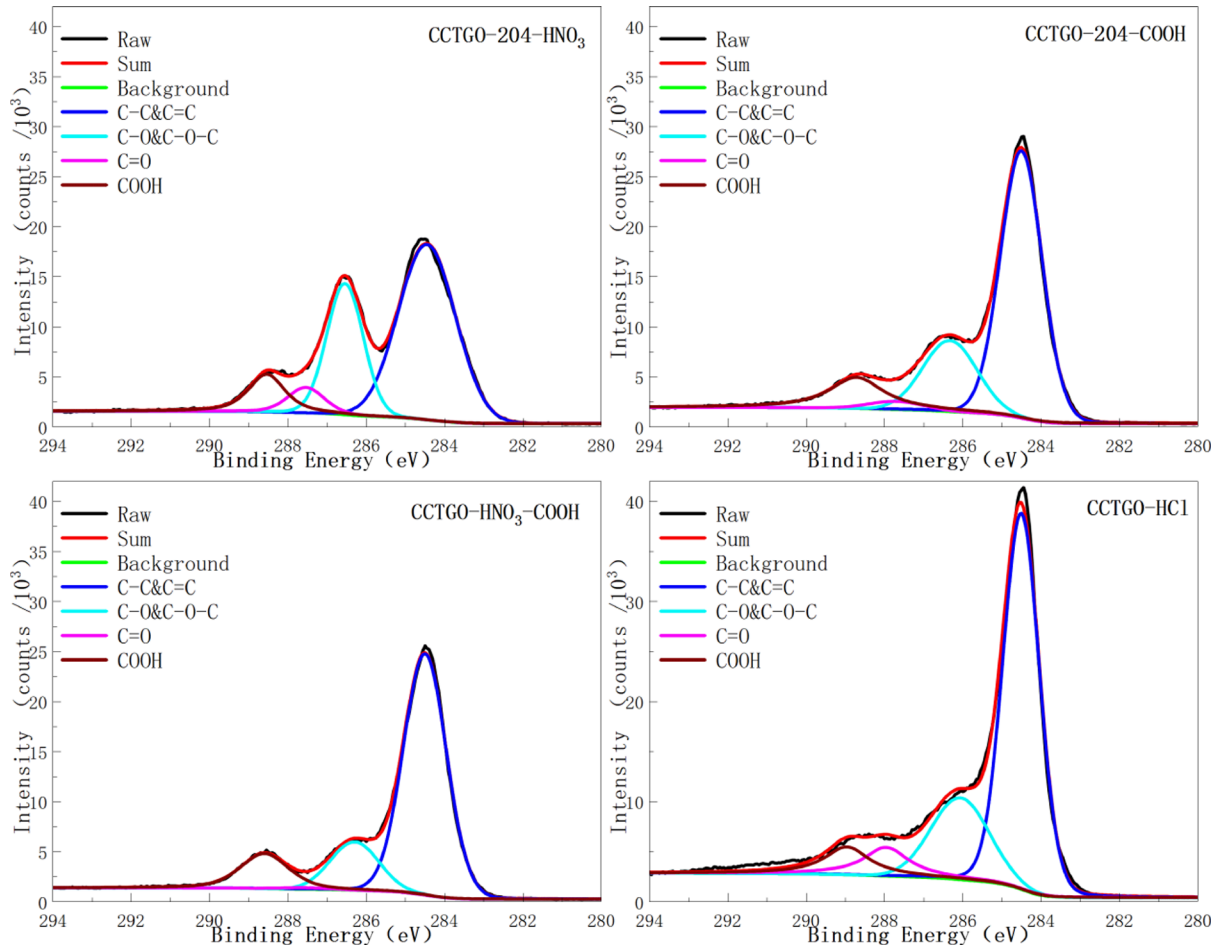

Figure 8. C 1s-XPS of the modified GO samples. Six kinds of carbon connection modes can be distinguished from C 1s-XPS spectra, including C−C, C═C, C−O, C−O−C, C═O, and O=C−OH. Fitting results show that the relative content of O═C−OH for the four original GO samples is CCTGO-204-HNO3-COOH > CCTGO-204-NO3 ≈ CCTGO-204-COOH > CCTGO-204-HCl. The relative contents of the sum of C−O and C−O−C are decreased for all modified samples compared with CCTGO-204.

removed during the modifications, which was also supported by the result of elemental analysis (the content of oxygen: CCTGO-204 > CCTGO-HNO_3 > CCTGO-204-HNO_3-COOH > CCTGO-204-COOH > CCTGO-204-HCl). Therefore, the modifications by concentrated HNO_3 can increase the content of proton-dissociable functional groups, while concentrated HCl cannot. Both these modifications cause the loss of epoxies, which significantly influence the dispersibilities of materials. Also, potentiometric titration can describe in detail the variation of proton-dissociable functional groups, which is also a useful characterization method for GOs.

4. CONCLUSIONS

In this work, we combined potentiometric titration and DFT calculation to identify the main oxygen-containing functional groups and their energy-favorable conformations on GO. A new GO model was proposed wherein the functional groups at the edges are mainly double-interactive carboxyls and double-adjacent phenolic hydroxyls, while the groups on the plane are mainly collocated epoxies and hydroxyls on both sides of the plane with meta-positional hydrogen bond interaction. Also, a solution was provided to acquire the accurate content of dissociable functional groups of GO in aqueous solutions, which is essential to the future research. In addition, a new method for accurate estimation of pK_a values for large molecular structures is provided.

■ ASSOCIATED CONTENT

Supporting Information

The Supporting Information is available free of charge at https://pubs.acs.org/doi/10.1021/acsomega.3c01596.

Details of conformation screening of hydroxyl and epoxy on the plane of GO, RCDPKA calculations, fitting results of GO titration, and experimental characterizations of GO samples (PDF)

■ AUTHOR INFORMATION

Corresponding Authors

Suliang Yang − *Department of Radiochemistry, China Institute of Atomic Energy, Beijing 102413, China;* orcid.org/0000-0002-4143-7618; Email: ysl79@ciae.ac.cn

Shengdong Zhang − *Department of Radiochemistry, China Institute of Atomic Energy, Beijing 102413, China;* Email: Zhangsd@ciae.ac.cn

Authors

Wuqing Tao − *Department of Radiochemistry, China Institute of Atomic Energy, Beijing 102413, China;* Present

https://doi.org/10.1021/acsomega.3c01596
ACS Omega 2023, 8, 24332−24340

Address: College of Science, Jiangxi Agricultural University, Nanchang 330045, China
Youshi Lan − *Department of Radiochemistry, China Institute of Atomic Energy, Beijing 102413, China*
Jiqiao Zhang − *Department of Radiochemistry, China Institute of Atomic Energy, Beijing 102413, China*
Liyang Zhu − *Department of Radiochemistry, China Institute of Atomic Energy, Beijing 102413, China*
Qian Liu − *Department of Radiochemistry, China Institute of Atomic Energy, Beijing 102413, China;* orcid.org/0000-0003-0762-8725
Yating Yang − *Department of Radiochemistry, China Institute of Atomic Energy, Beijing 102413, China*
Guoxin Tian − *Department of Radiochemistry, China Institute of Atomic Energy, Beijing 102413, China;* orcid.org/0000-0002-8755-0026

Complete contact information is available at: https://pubs.acs.org/10.1021/acsomega.3c01596

Author Contributions

W.T. and Y.L. contributed equally to this work. W.T. conducted the experimental titration. Y.L. performed the DFT calculations. J.Z., L.Z., Q.L., and Y.Y. analyzed the data and co-wrote this article. S.Y., G.T., and S.Z. directed the experiments and calculations. All authors participated in the discussion and modified the article.

Funding

This work was financially supported by the President Foundation of China Institute of Atomic Energy (No. YZ202212000903) and the Youth Talent Project of China National Nuclear Corporation (No. FC202212000103).

Notes

The authors declare no competing financial interest.

■ ACKNOWLEDGMENTS

Support from the Department of Radiochemistry of China Institute of Atomic Energy is highly appreciated.

■ REFERENCES

(1) Eigler, S.; Hirsch, A. Chemistry with Graphene and Graphene Oxide - Challenges for Synthetic Chemists. *Angew. Chem., Int. Ed.* **2014**, *53*, 7720−7738.
(2) Chen, D.; Feng, H.; Li, J. Graphene Oxide: Preparation, Functionalization, and Electrochemical Applications. *Chem. Rev.* **2012**, *112*, 6027−6053.
(3) Peng, W.; Li, H.; Liu, Y.; Song, S. A review on heavy metal ions adsorption from water by graphene oxide and its composites. *J. Mol. Liq.* **2017**, *230*, 496−504.
(4) Dong, L.; Yang, J.; Chhowalla, M.; Loh, K. P. Synthesis and reduction of large sized graphene oxide sheets. *Chem. Soc. Rev.* **2017**, *46*, 7306−7316.
(5) Dimiev, A. M.; Eigler, S. *Graphene Oxide: Fundamentals and Applications*; Wiley, 2016; pp 36−84.
(6) Gao, W. *Graphene Oxide*; Springer, 2015; pp 61−95.
(7) Brodie, B. C. Philos. XIII. On the atomic weight of graphite. *Trans. R. Soc. Lond.* **1859**, *149*, 249−259.
(8) Staudenmaier, L. J. R. Verfahren zur darstellung der graphitsäure. *Berichte der deutschen chemischen Gesellschaft* **1898**, *31*, 1481−1487.
(9) Hofmann, U.; König, E. Untersuchungen über graphitoxyd. *Zeitschrift für anorganische und allgemeine Chemie* **1937**, *234*, 311−336.
(10) Hummers, W. S.; Offeman, R. E. Preparation of graphitic oxide. *J. Am. Chem. Soc.* **1958**, *80*, 1339.
(11) Marcano, D. C.; Kosynkin, D. V.; Berlin, J. M.; Sinitskii, A.; Sun, Z.; Slesarev, A.; Alemany, L. B.; Lu, W.; Tour, J. M. Improved synthesis of graphene oxide. *ACS Nano* **2010**, *4*, 4806−4814.
(12) Hofmann, U.; Holst, R. Über die Säurenatur und die Methylierung von Graphitoxyd. *Ber. Dtsch. Chem. Ges.* **1939**, *72*, 754−771.
(13) Mkhoyan, K. A.; Contryman, A. W.; Silcox, J.; Stewart, D. A.; Eda, G.; Mattevi, C.; Miller, S.; Chhowalla, M. Atomic and electronic structure of graphene-oxide. *Nano Lett.* **2009**, *9*, 1058−1063.
(14) Scholz, W.; Boehm, H.-P. Z. Formation process and structure of graphite oxide. *Anorg. Allg. Chem.* **1969**, *369*, 327−340.
(15) Nakajima, T.; Matsuo, Y. Formation process and structure of graphite oxide. *Carbon* **1994**, *32*, 469−475.
(16) Lerf, A.; He, H. Y.; Forster, M.; Klinowski, J. Structure of graphite oxide revisited. *J. Phys. Chem. B* **1998**, *102*, 4477−4482.
(17) Szabó, T.; Berkesi, O.; Forgó, P.; Josepovits, K.; Sanakis, Y.; Petridis, D.; Dékány, I. Evolution of surface functional groups in a series of progressively oxidized graphite oxides. *Chem. Mater.* **2006**, *18*, 2740−2749.
(18) Brisebois, P. P.; Siaj, M. Harvesting graphene oxide − years 1859 to 2019: a review of its structure, synthesis, properties and exfoliation. *J. Mater. Chem. C* **2020**, *8*, 1517−1547.
(19) Cai, W.; Piner, R. D.; Stadermann, F. J.; Park, S.; Shaibat, M. A.; Ishii, Y.; Yang, D.; Velamakanni, A.; An, S. J.; Stoller, M.; An, J.; Chen, D.; Ruoff, R. S. Synthesis and Solid-State NMR Structural Characterization of 13C-Labeled Graphite Oxide. *Science* **2008**, *321*, 1815−1817.
(20) Chen, D.; Feng, H.; Li, J. Graphene oxide: preparation, functionalization, and electrochemical applications. *Chem. Rev.* **2012**, *112*, 6027−6053.
(21) Peng, Y.-Y.; Liu, Y.-M.; Chang, J.-K.; Wu, C.-H.; Ger, M.-D.; Pu, N.-W.; Chang, C.-L. A facile approach to produce holey graphene and its application in supercapacitors. *Carbon* **2015**, *81*, 347−356.
(22) Saxena, S.; Tyson, T. A.; Negusse, E. Investigation of the local structure of graphene oxide. *J. Phys. Chem. Lett.* **2010**, *1*, 3433−3437.
(23) Pacilé, D.; Meyer, J. C.; Fraile Rodríguez, A.; Papagno, M.; Gómez-Navarro, C.; Sundaram, R. S.; Burghard, M.; Kern, K.; Carbone, C.; Kaiser, U. Electronic properties and atomic structure of graphene oxide membranes. *Carbon* **2011**, *49*, 966−972.
(24) Bagri, A.; Mattevi, C.; Acik, M.; Chabal, Y. J.; Chhowalla, M.; Shenoy, V. B. Structural evolution during the reduction of chemically derived graphene oxide. *Nat. Chem.* **2010**, *2*, 581−587.
(25) Lee, V.; Whittaker, L.; Jaye, C.; Baroudi, K. M.; Fischer, D. A.; Banerjee, S. Large-Area Chemically Modified Graphene Films: Electrophoretic Deposition and Characterization by Soft X-ray Absorption Spectroscopy. *Chem. Mater.* **2009**, *21*, 3905−3916.
(26) Yang, J.; Shi, G.; Tu, Y.; Fang, H. High Correlation between Oxidation Loci on Graphene Oxide. *Angew. Chem., Int. Ed.* **2014**, *53*, 10190−1019410358.
(27) Mouhat, F.; Coudert, F. X.; Bocquet, M. L. Structure and chemistry of graphene oxide in liquid water from first principles. *Nat. Commun.* **2020**, *11*, 1566−1569.
(28) Kornilov, D. Y.; Gubin, S. P. Graphene oxide: Structure, properties, synthesis, and reduction (a review). *Russ. J. Inorg. Chem.* **2020**, *65*, 1965−1976.
(29) Chen, L.; Shi, G.; Shen, J.; Peng, B.; Zhang, B.; Wang, Y.; Bian, F.; Wang, J.; Li, D.; Qian, Z.; Xu, G.; Liu, G.; Zeng, J.; Zhang, L.; Yang, Y.; Zhou, G.; Wu, M.; Jin, W.; Li, J.; Fang, H. Ion sieving in graphene oxide membranes via cationic control of interlayer spacing. *Nature* **2017**, *550*, 380−383.
(30) Gans, P.; Sabatini, A.; Vacca, A. Investigation of equilibria in solution. Determination of equilibrium constants with the HYPERQUAD suite of programs. *Talanta* **1996**, *43*, 1739−1753.
(31) Becke, A. D. Density-functional thermochemistry. III. The role of exact exchange. *J. Chem. Phys.* **1993**, *98*, 5648−5652.
(32) Lee, C.; Yang, W.; Parr, R. G. Development of the Colle-Salvetti correlation-energy formula into a functional of the electron density. *Phys. Rev. B: Condens. Matter* **1988**, *37*, 785−789.

(33) Schäfer, A.; Horn, H.; Ahlrichs, R. Fully optimized contracted Gaussian basis sets for atoms Li to Kr. *J. Chem. Phys.* **1992**, *97*, 2571−2577.
(34) Schäfer, A.; Huber, C.; Ahlrichs, R. Fully optimized contracted Gaussian basis sets of triple zeta valence quality for atoms Li to Kr. *J. Chem. Phys.* **1994**, *100*, 5829−5835.
(35) Frisch, M. J.; Trucks, G. W.; Schlegel, H. B.; Scuseria, G. E.; Robb, M. A.; Cheeseman, J. R.; Scalmani, G.; Barone, V.; Mennucci, B.; Petersson, G. A.; Nakatsuji, H.; Caricato, M.; Li, X.; Hratchian, H. P.; Izmaylov, A. F.; Bloino, J.; Zheng, G.; Sonnenberg, J. L.; Hada, M.; Ehara, M.; Toyota, K.; Fukuda, R.; Hasegawa, J.; Ishida, M.; Nakajima, T.; Honda, Y.; Kitao, O.; Nakai, H.; Vreven, T.; Montgomery, J. A., Jr.; Peralta, J. E.; Ogliaro, F.; Bearpark, M.; Heyd, J. J.; Brothers, E.; Kudin, K. N.; Staroverov, V. N.; Keith, T.; Kobayashi, R.; Normand, J.; Raghavachari, K.; Rendell, A.; Burant, J. C.; Iyengar, S. S.; Tomasi, J.; Cossi, M.; Rega, N.; Millam, J. M.; Klene, M.; Knox, J. E.; Cross, J. B.; Bakken, V.; Adamo, C.; Jaramillo, J.; Gomperts, R.; Stratmann, R. E.; Yazyev, O.; Austin, A. J.; Cammi, R.; Pomelli, C.; Ochterski, J. W.; Martin, R. L.; Morokuma, K.; Zakrzewski, V. G.; Voth, G. A.; Salvador, P.; Dannenberg, J. J.; Dapprich, S.; Daniels, A. D.; Farkas, O.; Foresman, J. B.; Ortiz, J. V.; Cioslowski, J.; Fox, D. J. *Gaussian 09*; Gaussian, Inc.: Wallingford, CT, 2009; Vol. *121*; pp 150−166.
(36) Marenich, A. V.; Cramer, C. J.; Truhlar, D. G. Universal Solvation Model Based on Solute Electron Density and on a Continuum Model of the Solvent Defined by the Bulk Dielectric Constant and Atomic Surface Tensions. *J. Phys. Chem. B* **2009**, *113*, 6378−6396.
(37) Ehrlich, S.; Moellmann, J.; Reckien, W.; Bredow, T.; Grimme, S. System-dependent dispersion coefficients for the DFT-D3 treatment of adsorption processes on ionic surfaces. *Chem. Phys. Chem.* **2011**, *12*, 3414−3420.
(38) Bellunato, A.; Arjmandi Tash, H.; Cesa, Y.; Schneider, G. F. Chemistry at the Edge of Graphene. *ChemPhysChem* **2016**, *17*, 785−801.
(39) Denis, P. A.; Iribarne, F. Comparative study of defect reactivity in graphene. *J. Phys. Chem. C* **2013**, *117*, 19048−19055.
(40) Denis, P. A.; Iribarne, F. Monolayer and bilayer graphene functionalized with nitrene radicals. *J. Phys. Chem. C* **2011**, *115*, 195−203.
(41) Shi, L.; Ying, Z.; Xu, A.; Cheng, Y. Unraveling the water-mediated proton conduction mechanism along the surface of graphene oxide. *Chem. Mater.* **2020**, *32*, 6062−6069.
(42) Tu, Y.; Zhao, L.; Sun, J.; Wu, Y.; Zhou, X.; Chen, L.; Lei, X.; Fang, H.; Shi, G. Water-Mediated Spontaneously Dynamic Oxygen Migration on Graphene Oxide with Structural Adaptivity for Biomolecule Adsorption. *Chinese Phys. Lett.* **2020**, *37*, 066803.
(43) Kelly, C. P.; Cramer, C. J.; Truhlar, D. G. Aqueous solvation free energies of ions and ion− water clusters based on an accurate value for the absolute aqueous solvation free energy of the proton. *J. Phys. Chem. B* **2006**, *110*, 16066−16081.
(44) Liu, S.; Pedersen, L. G. Estimation of molecular acidity via electrostatic potential at the nucleus and valence natural atomic orbitals. *J. Phys. Chem. A* **2009**, *113*, 3648−3655.
(45) Olsson, M. H. M.; Søndergaard, C. R.; Rostkowski, M.; Jensen, J. H. PROPKA3: Consistent Treatment of Internal and Surface Residues in Empirical pKa Predictions. *J. Chem. Theory Comput.* **2011**, *7*, 525−537.
(46) Anandakrishnan, R.; Aguilar, B.; Onufriev, A. V. H++ 3.0: automating pK prediction and the preparation of biomolecular structures for atomistic molecular modeling and simulations. *Nucleic Acids Res.* **2012**, *40*, 537−541.
(47) Zeng, Y.; Chen, X.; Zhao, D.; Li, H.; Zhang, Y.; Xiao, X. Estimation of pKa values for carboxylic acids, alcohols, phenols and amines using changes in the relative Gibbs free energy. *Fluid Phase Equilib.* **2012**, *313*, 148−155.

https://doi.org/10.1021/acsomega.3c01596
ACS Omega 2023, 8, 24332−24340